Multistage Sampling Structure Conversion of Video Signals

R. Manduchi, G. M. Cortelazzo, and G. A. Mian

Abstract—**This work extends multistage implementation of sampling structure conversion to the multidimensional (M-D) case. The issues arising in this task are usefully addressed on the basis of lattice theory.**

Numerical data supporting the advantages of multistage sampling conversion are presented, and the case of format conversion from 4/3 to 16/9 aspect ratio is examined as a study case.

The main indication of this work is that multistage implementation, in the case of systems for sampling structure conversion of video signals, may improve the system characteristics and visual rendition.

I. Introduction

A growing number of applications in the area of improved quality television (IQTV) and high definition television (HDTV) call for sampling structure conversion of television signals.

Examples of such occurrences are the conversion from a scanning standard to a different one (rather typical is so-called deinterlacing, i.e., the conversion from interlaced to progressive scanning standard), the format conversion from 4/3 to 16/9 aspect ratio, and the zooming of a scene's details for the picture-in-picture feature. All these applications require practical and effective sampling structure conversion techniques.

A one-dimensional (1-D) signal with sampling period T_1 can be conveniently converted into a signal with sampling period T_2 by a well-known three-step procedure [1] if $T_2/T_1 = M/L$, with M and L coprime integers. The first step of such a procedure (up-sampling) decreases the input signal sampling period to T_2/L (by suitable zero padding). The second step performs an appropriate low-pass filtering of the signal sampled at T_1/L. The third step (down-sampling) decimates the low-pass filtered signal at sampling period T_2. When T_2/T_1 is not rational, or when L is very large, the sampling rate conversion can be effectively performed by methods of the type proposed in [9].

The procedure of [1] has been extended to the case of multidimensional (M-D) signals in [3] and [2]. Its practical application for changing a signal defined on lattice Λ_1 into a signal defined on lattice Λ_2 requires the determination of their sum [2], as well as the devising of filter specifications suitable to the undertaken task.

The procedure of [3] and [2] is appropriate for situations where the ratio between the density of the sum of two lattices and the density of one of them is not too large. A method for determining such a ratio without explicitely determining the sum of two lattices is another useful result of this work.

The computational and/or performance advantages of the multistage implementation of 1-D sampling rate converters are well known [1]. Their theoretical justification rests upon the relationship between transition bandwidth and minimax error for the 1-D linear phase FIR filters.

This work examines in detail the implications of multistage implementation of M-D sampling rate converters, originally proposed in [19] and [12], which in many cases have no 1-D counterpart. Multistage implementation is shown to be advantageous also in the case of M-D sampling structure conversion. The theoretical characterization of such advantages is considerably more difficult than in the 1-D case for various reasons.

The theory of FIR filters, in the M-D case, is not yet understood as well as in the 1-D case. The relationships between M-D FIR filter orders and their transition bands are not known. Hence the arguments justifying the performance gains of 1-D multistage implementation (when the considered performance parameter is the minimax error) cannot be easily extended to the M-D case. Some conjectures grounded on experimental data motivate the minimax error gains of M-D multistage schemes.

In the case of video filters, the minimax error of the system frequency response is not as significant as in the 1-D case. Other parameters, such as the passband smoothness of the frequency response [31] and the step-response behavior ("ringing") [32], are also very important for visual rendition. The analytical relationships between such parameters and multistage implementation would be very difficult to express also in the case of 1-D systems. Although no clear theoretical argument is presently available to justify the general characteristics of multistage implementation of M-D systems, the presented data show that their overall performance is extremely interesting for video applications.

The M-D multistage implementation theory is exemplified by using format conversion from 4/3 to 16/9 aspect ratio as a study case. This application is of considerable interest in current television practice.

Manuscript received June 17, 1992; revised January 8, 1993 and April 19, 1993. This work was supported by CNR-Progetto Finalizzato Telecomunicazioni under Contract 91.01819.PF71. Paper was recommended by Associate Editor Yrjö Neuvo.

The authors are with the Dipartimento di Elettronica ed Informatica, 35131 Padova, Italy.

IEEE Log Number 9211202.

Although this issue is not treated in this work, it is worth noting that the presented M-D multistage implementation theory can also be applied to M-D IFIR filters [12], [19].

This paper has five sections. Topics concerning M-D sampling rate conversion require familiarity with lattice theory. Some essential notions are presented in the Appendix and some more advanced concepts in Subsections II-A and II-B. Subsection II-C discusses the M-D sampling structure conversion scheme of [2] and [3] and some practical aspects of its application. Section III introduces multistage implementation of M-D systems. Section IV applies the concepts of Section III to format conversion as a study case. Section V contains the conclusions.

II. Sampling Structure Conversion: Definitions and Fundamentals

The sampling rate conversion procedure of [1] has been extended to the case of M-D signals by [3] and [2]. Since M-D signals in the applications of most typical interest are defined on lattices, the presentation of some results concerning lattice theory serves as useful introduction to the procedure of [3] and [2].

A. Some Lattice Theory Results

This subsection assumes familiarity with basic matrix theory notions and results. For the reader's convenience, the necessary background is summarized in the Appendix.

Let $\mathbb{Z}_M$, $\mathbb{Q}_M$, and $\mathbb{R}_M$ denote the rings of the $M \times M$ matrixes with integer, rational, and real entries, respectively.

Given integers l and m, if there is an integer n such that $l = mn$, then m is said to divide l (written $m|l$).

Given $a \in \mathbb{Q}$, $\mathrm{den}(a)$ denotes the least positive integer such that $(\mathrm{den}(a) \cdot a) \in \mathbb{Z}$. Similarly, given matrix $\boldsymbol{A} \in \mathbb{Q}_M$, $\mathrm{den}(\boldsymbol{A})$ will denote the least positive integer such that $(\mathrm{den}(\boldsymbol{A}) \cdot \boldsymbol{A}) \in \mathbb{Z}_M$, that is, $\mathrm{den}(\boldsymbol{A})$ is the least common multiple among $\{\mathrm{den}(a_{ij})\}$, where a_{ij} are the entries of $\boldsymbol{A}$.

Let us recall that the M-dimensional lattice generated by basis $\boldsymbol{A} \in \mathbb{R}_M$ with nonsingular $\boldsymbol{A}$ (written $\mathrm{LAT}(\boldsymbol{A})$) is defined as set $\{\boldsymbol{a} = \boldsymbol{An},\ \boldsymbol{n} \in \mathbb{Z}^M\}$. Equivalently, a lattice can be defined as a discrete commutative subgroup of $\mathbb{R}^M$ [5]. Value $|\det(\boldsymbol{A})|$ is called the module of $\mathrm{LAT}(\boldsymbol{A})$, and its inverse represents the density of the points of $\mathrm{LAT}(\boldsymbol{A})$ [4].

Two fundamental results about lattices are reported below (for the proofs, see [4], [5], and [7]).

Result 1: Matrixes $\boldsymbol{A} \in \mathbb{R}_M$ and $\boldsymbol{B} \in \mathbb{R}_M$ are bases of the same lattice if and only if $\boldsymbol{A} = \boldsymbol{BU}$, with $\boldsymbol{U}$ the unimodular matrix of $\mathbb{Z}_M$. ■

Result 2: Given $\Lambda = \mathrm{LAT}(\boldsymbol{A})$ and $\Gamma = \mathrm{LAT}(\boldsymbol{B})$, Λ is a (proper) sublattice of Γ if and only if $\boldsymbol{A} = \boldsymbol{BH}$, with $\boldsymbol{H}$ full rank matrix of $\mathbb{Z}_M$ with $|\det(\boldsymbol{H})| > 1$. ■

Integer $|\det(\boldsymbol{H})|$ is called the index of Λ in Γ (denoted as $(\Gamma{:}\Lambda)$). It represents the ratio between the module of Λ and the module of Γ (that is, the ratio between the density of the points of Γ and the density of the points of Λ).

From Result 1, Result 2, and the Smith normal form theorem (Result A.2 of the Appendix), it can be seen that for an M-dimensional lattice Λ and an M-dimensional sublattice Γ of Λ, there exists a basis $\boldsymbol{A}$ of Λ and a basis $\boldsymbol{B}$ of Γ, whose vectors are pairwise parallel.

The next corollary [13] follows from Result 1 and Result 2.

Result 3: Given $k \in \mathbb{Z}$, let $(\boldsymbol{L}_i,\ i = 1,2,\cdots,n(k))$ be the set of Hermite normal form matrixes of $\mathbb{Z}_M$ with determinant equal to k. For a given M-dimensional lattice $\Lambda = \mathrm{LAT}(\boldsymbol{A})$, matrixes $\boldsymbol{AL}_i$, $i = 1,2,\cdots,n(k)$ are the bases of each and every M-dimensional sublattice of Λ with index k in Λ. ■

Given two M-dimensional lattices Λ_1 and Λ_2, their sum $\Lambda_1 + \Lambda_2$ is defined as

$$\Lambda_1 + \Lambda_2 = \{\boldsymbol{a} + \boldsymbol{b}\colon \boldsymbol{a} \in \Lambda_1, \boldsymbol{b} \in \Lambda_2\}. \tag{1}$$

The sum of two lattices is not necessarily a lattice; for instance, the sum of $\Lambda_1 = \{n \in \mathbb{Z}\}$ and $\Lambda_2 = \{n\sqrt{2},\ n \in \mathbb{Z}\}$ is not a 1-D lattice, since it is not a discrete group. The following lemma characterizes the sum of two lattices with basis in $\mathbb{R}_M$.

Lemma 1: Given M-dimensional lattices Λ_1 and Λ_2, $\Lambda_1 + \Lambda_2$ is an M-dimensional lattice if and only if there exists an M-dimensional lattice Ψ containing both Λ_1 and Λ_2. In such a case, $\Lambda_1 + \Lambda_2$ is the smallest lattice containing both Λ_1 and Λ_2 (the "smallest" means "the one with maximum module").

Proof: Since $\Lambda_1 + \Lambda_2$ contains both Λ_1 and Λ_2, is it necessary only to prove that if there exists a lattice Ψ such that

$$\Lambda_1 \subset \Psi \quad \text{and} \quad \Lambda_2 \subset \Psi \tag{2}$$

then $\Lambda_1 + \Lambda_2$ is a lattice. It is straightforward that every lattice Ψ satisfying (2.2) contains $\Lambda_1 + \Lambda_2$ and that $\Lambda_1 + \Lambda_2$ is a commutative subgroup of $\mathbb{R}^M$ (since Ψ, Λ_1, and Λ_2 are commutative subgroups of $\mathbb{R}^M$). Hence $\Lambda_1 + \Lambda_2$ is a lattice (as Ψ is discrete and finite-dimensional); actually, it is the intersection among all the lattices containing both Λ_1 and Λ_2. Since the module of the intersection between two lattices is greater than, or equal to, the maximum between the modules of the two lattices, $\Lambda_1 + \Lambda_2$ is the lattice with the maximum module among the lattices containing both Λ_1 and Λ_2. ■

A theorem characterizing the basis of the sum of two lattices with bases in $\mathbb{R}_M$ (if the sum is a lattice) follows. The procedure uses the notion of greatest common left divisor (gcld) of two matrixes, which can be found in the Appendix.

Theorem 1: Given $\Lambda_1 = \mathrm{LAT}(\boldsymbol{A})$ and $\Lambda_2 = \mathrm{LAT}(\boldsymbol{C})$, with $\boldsymbol{A}, \boldsymbol{C} \in \mathbb{R}_M$, $\Lambda_1 + \Lambda_2$ is a lattice if and only if $\boldsymbol{A}^{-1}\boldsymbol{C} \in \mathbb{Q}_M$. If $\Lambda_1 + \Lambda_2$ is a lattice, it is $\Lambda_1 + \Lambda_2 = \mathrm{LAT}(\mathrm{gcld}(\boldsymbol{A}, \boldsymbol{C}))$.

Proof: If $\Lambda_1 + \Lambda_2$ is a lattice, then a basis $\boldsymbol{B} \in \mathbb{R}_M$ of $\Lambda_1 + \Lambda_2$ exists. Both Λ_1 and Λ_2 are sublattices of $\Lambda_1 + \Lambda_2$ and, by Result 2, there exists a pair of full rank

matrixes $\boldsymbol{H}$ and $\boldsymbol{K}$ of $\mathbb{Z}_M$ such that

$$\boldsymbol{A} = \boldsymbol{BH} \quad \text{and} \quad \boldsymbol{C} = \boldsymbol{BK}. \tag{3}$$

From the equalities above it follows that $\boldsymbol{B} = \boldsymbol{AH}^{-1} = \boldsymbol{CK}^{-1}$ and

$$\boldsymbol{A}^{-1}\boldsymbol{C} = \boldsymbol{H}^{-1}\boldsymbol{K} \tag{4}$$

Hence, if $\Lambda_1 + \Lambda_2$ is a lattice, then $\boldsymbol{A}^{-1}\boldsymbol{C} \in \mathbb{Q}_M$.

The proof that if $\boldsymbol{A}^{-1}\boldsymbol{C} \in \mathbb{Q}_M$ then $\Lambda_1 + \Lambda_2 = \mathrm{LAT}(\mathrm{gcld}(\boldsymbol{A}, \boldsymbol{C}))$ is a simple generalization of a result contained in [33]. ■

If $\Lambda = \mathrm{LAT}(\boldsymbol{A})$, $\Lambda^* = \mathrm{LAT}(\boldsymbol{A}^{-T})$ is the reciprocal lattice of Λ [2]. It should be noted that the procedure for determining a basis of the sum of two lattices can also be used for determining a basis of the intersection of two lattices, in force of the result [2]

$$\Lambda_1^* \cap \Lambda_2^* = (\Lambda_1 + \Lambda_2)^* \tag{5}$$

A procedure for directly determining a basis of $\Lambda_1 \cap \Lambda_2$, when Λ_1 and Λ_2 have bases in $\mathbb{Z}_M$, is given in [11].

The following corollary allows one to obtain the value of $(\Lambda_1 + \Lambda_2{:}\Lambda_1)$ (or $(\Lambda_1 + \Lambda_2{:}\Lambda_2)$) without explicitly finding a basis for $\Lambda_1 + \Lambda_2$, when Λ_1 and Λ_2 are two-dimensional lattices.

Corollary 1: Given $\Lambda_1 = \mathrm{LAT}(\boldsymbol{A})$ and $\Lambda_2 = \mathrm{LAT}(\boldsymbol{C})$, with $\boldsymbol{A}, \boldsymbol{C} \in \mathbb{R}_2$, if $\Lambda_1 + \Lambda_2$ is a lattice the following equalities hold:

$$(\Lambda_1 + \Lambda_2{:}\Lambda_1) = \mathrm{den}(\boldsymbol{A}^{-1}\boldsymbol{C}) \cdot \mathrm{den}(\mathrm{den}(\boldsymbol{A}^{-1}\boldsymbol{C}) \cdot \det(\boldsymbol{A}^{-1}\boldsymbol{C})) \tag{6}$$

$$(\Lambda_1 + \Lambda_2{:}\Lambda_2) = \mathrm{den}(\boldsymbol{A}^{-1}\boldsymbol{C}) \cdot \det(\boldsymbol{A}^{-1}\boldsymbol{C}) \cdot \mathrm{den}(\mathrm{den}(\boldsymbol{A}^{-1}\boldsymbol{C}) \cdot \det(\boldsymbol{A}^{-1}\boldsymbol{C})) \tag{7}$$

Proof: It follows directly from Theorem 1 and Corollary A.1. ■

As an example of application of Corollary 1, consider the design of a transcoder from CCIR System I standard 525/2:1/60 to CCIR System M standard 625/2:1/50. Call Λ_1 the verticotemporal lattice corresponding to the System I raster and Λ_2 the verticotemporal lattice corresponding to the System M raster. As will be explained in the next section, a possible transcoder scheme required operation in $\Lambda_1 + \Lambda_2$. A basis of Λ_1 is

$$\boldsymbol{A} = \begin{pmatrix} \frac{1}{30} & \frac{1}{60} \\ 0 & \frac{1}{525} \end{pmatrix},$$

and a basis of Λ_2 is

$$\boldsymbol{C} = \begin{pmatrix} \frac{1}{25} & \frac{1}{50} \\ 0 & \frac{1}{625} \end{pmatrix}.$$

Since

$$\boldsymbol{A}^{-1}\boldsymbol{C} = \begin{pmatrix} \frac{6}{5} & \frac{9}{50} \\ 0 & \frac{21}{25} \end{pmatrix},$$

$$\det(\boldsymbol{A}^{-1}\boldsymbol{C}) = \frac{126}{125}, \quad \mathrm{den}(\boldsymbol{A}^{-1}\boldsymbol{C}) = 50.$$

By Corollary 1 it is $(\Lambda_1 + \Lambda_2{:}\Lambda_1) = 250$, a notion which can be profitably exploited in order to devise practical transcoder schemes, as Subsection C explains.

B. Descending and Ascending Lattice Chains

Since multistage implementation has received a lot of attention in the 1-D case, the possibility of changing sampling structure from M-dimensional lattice Γ to M-dimensional lattice Λ, with $\Gamma \supset \Lambda$, in p intermediate steps concerning lattices $\Psi_1, \Psi_2, \cdots, \Psi_{p-1}$ such that $\Gamma \supset \Psi_1 \supset \Psi_2 \supset \cdots \supset_{p-1} \Psi \supset \Lambda$, deserves special attention.

Let $\mathscr{A} = (\alpha_1, \alpha_2, \cdots, \alpha_p)$ be any ordered decomposition of $(\Gamma{:}\Lambda)$ into positive integer factors:

i) $\alpha_i \in \mathbb{Z}, \quad \alpha_i > 0, \quad i = 1, 2, \cdots, p$

ii) $\alpha_1 \alpha_2 \cdots \alpha_p = (\Gamma{:}\Lambda)$ (8)

Any ordered set of M-dimensional lattices $(\Psi_1, \Psi_2, \cdots, \Psi_{p-1})$ such that

i) $\Gamma \supset \Psi_1 \supset \Psi_2 \supset \cdots \supset \Psi_{p-1} \supset \Lambda$

ii) $(\Gamma{:}\Psi_1) = \alpha_1; \quad (\Psi_{i-1}{:}\Psi_i) = \alpha_i, \quad 1 < i < p; \quad (\Psi_{p-1}{:}\Lambda) = \alpha_p$ (9)

will be called a descending lattice chain (dlc) on $\mathscr{A}$ from Γ to Λ.

Given $\mathscr{A} = (\alpha_1, \alpha_2, \cdots, \alpha_p)$, $\Gamma = \mathrm{LAT}(\boldsymbol{P})$ and $\Lambda = \mathrm{LAT}(\boldsymbol{Q})$, with $\Gamma \supset \Lambda$, let one call $\boldsymbol{H} = \boldsymbol{P}^{-1}\boldsymbol{Q}$ ($\boldsymbol{H} \in \mathbb{Z}_M$ by Result 2). An algorithm for finding all the dlc on $\mathscr{A}$ from Γ to Λ may be represented by an oriented graph, where each node corresponds to a lattice. The graph is organized in $(p + 1)$ levels. At level 0 there is a single node, corresponding to lattice Γ. Such a node branches into the nodes of level 1. Each one of these nodes corresponds to one of the n_1 sublattices $\{\Psi_{1,i} = \mathrm{LAT}(\boldsymbol{PM}_{1,i}), i = 1, 2, \cdots, n_1\}$ of Γ with index equal to α_1. From Result 3, it can be assumed that matrixes $\boldsymbol{M}_{1,i}$ are in Hermite normal form.

Each lattice at level 1 is connected to all its sublattices with an index equal to α_2, forming the nodes of level 2. The graph is built by iterating such a procedure for $i = 3, 4, \cdots p$. The bases of all (and only) the ith level lattices are matrixes $\boldsymbol{PM}_1\boldsymbol{M}_2 \cdots \boldsymbol{M}_i$, with $\boldsymbol{M}_j \in \mathbb{Z}_M$ Hermite normal form matrix such that $\det(\boldsymbol{M}_j) = \alpha_j$.

Note that according to (9), the pth level necessarily includes lattice Λ. Such a fact implies that each dlc on $\mathscr{A}$ from Γ to Λ is associated to an oriented path from Γ to Λ. Therefore, the determination of all the dlc on $\mathscr{A}$ from Γ to Λ is equivalent to the determination of all the sequences of Hermite normal form matrixes $(\boldsymbol{M}_1, \boldsymbol{M}_2, \cdots,$

M_p) of $\mathbb{Z}_M$ with $\det(M_i) = \alpha_i$, such that $M_1 M_2 \cdots M_p$ is right equivalent to H. Note that $PM_1 M_2 \cdots M_p$ is a basis of Λ (because it is right-equivalent to Q).

The determination of $(M_1, M_2, \cdots, M_p)$, with $\det(M_i) = \alpha_i$, $i = 1, 2, \cdots, p$, such that $M_1 M_2 \cdots M_p$ is right-equivalent to H, just requires the finding of $p - 1$ matrixes $(M_1, M_2, \cdots, M_{p-1})$ such that $(M_1 M_2 \cdots M_{p-1})^{-1} H = G$ belongs to $\mathbb{Z}_M$. Matrix M_p is, indeed, the Hermite normal form matrix right-equivalent to G. It should be noted that the determination of such matrixes $M_1, M_2, \cdots, M_p$ can be accomplished by a trial and error procedure of the above-sketched type.

By Result A.3 of the Appendix, given Γ, Λ, and $\mathscr{A}$, there exists at least one dlc on $\mathscr{A}$ from Γ to Λ. It should be clear, as the following example shows, that given Γ, Λ, and $\mathscr{A}$, there may be more than one dlc on $\mathscr{A}$ from Γ to Λ. Consider, for instance, $\Gamma = \mathrm{LAT}(P)$ and $\Lambda = \mathrm{LAT}(Q)$,

$$P = \begin{pmatrix} 1 & 0 \\ 0 & 1 \end{pmatrix} \qquad Q = \begin{pmatrix} 4 & 2 \\ 0 & 2 \end{pmatrix}$$

and let

$$H = P^{-1}Q = \begin{pmatrix} 4 & 2 \\ 0 & 2 \end{pmatrix}.$$

It is $(\Gamma{:}\Lambda) = |\det(H)| = 8$. Let one, for instance, choose $\mathscr{A} = (2, 2, 2)$. The Hermite normal form matrixes of $\mathbb{Z}_2$ with determinant equal to 2 are

$$V_1 = \begin{pmatrix} 2 & 0 \\ 0 & 1 \end{pmatrix} \qquad V_2 = \begin{pmatrix} 2 & 1 \\ 0 & 1 \end{pmatrix} \qquad V_3 = \begin{pmatrix} 1 & 0 \\ 0 & 2 \end{pmatrix}$$

It is easy to see that $(V_m V_n)^{-1} H \in \mathbb{Z}_2$ only if $(m = 1, n = 3)$, $(m = 2, n = 1)$, $(m = 2, n = 2)$, $(m = 2, n = 3)$, or $(m = 3, n = 1)$. Therefore, there are just five distinct dlc's on $\mathscr{A}$ from Γ to Λ, namely

$$(\mathrm{LAT}(\mathbf{PV}_1), \mathrm{LAT}(\mathbf{PV}_1\mathbf{V}_3)), \quad (\mathrm{LAT}(\mathbf{PV}_2), \mathrm{LAT}(\mathbf{PV}_2\mathbf{V}_1)),$$
$$(\mathrm{LAT}(\mathbf{PV}_2), \mathrm{LAT}(\mathbf{PV}_2\mathbf{V}_2)), \quad (\mathrm{LAT}(\mathbf{PV}_2), \mathrm{LAT}(\mathbf{PV}_2\mathbf{V}_3)),$$
$$(\mathrm{LAT}(\mathbf{PV}_3), \mathrm{LAT}(\mathbf{PV}_3\mathbf{V}_1)). \qquad (10)$$

The five possibilities are shown in Fig. 1 (the paths of the graph not leading to Λ are not shown, for clarity's sake). The arrowed lines indicate matrix multiplication of the lattice basis by the matrixes written next to them. The lattices of each dlc are explicitely shown in the figure.

The passage from Λ to Γ can be similarly handled by ascending lattice chains (alc's), i.e., by any ordered set of lattices $\Phi_1, \Phi_2, \cdots, \Phi_{p-1}$ such that

i) $\Gamma \subset \Phi_1 \subset \Phi_2 \subset \cdots \subset \Phi_{p-1} \subset \Lambda$

ii) $(\Phi_1{:}\Gamma) = \alpha_1$; $(\Phi_i{:}\Phi_{i-1}) = \alpha_i$, $1 < i < p$;
$(\Lambda{:}\Phi_{p-1}) = \alpha_p$ (11)

The determination of all the alc's on $\mathscr{A}$ from Λ to Γ is equivalent to the determination of all the sequences of Hermite normal form matrixes $(L_0, L_1, \cdots, L_{p-1})$ of $\mathbb{Z}_M$ with $\det(L_i) = \alpha_i$. Then, a basis D_i of Φ_i is $D_i = PL_{p-1}L_{p-2} \cdots L_i$.

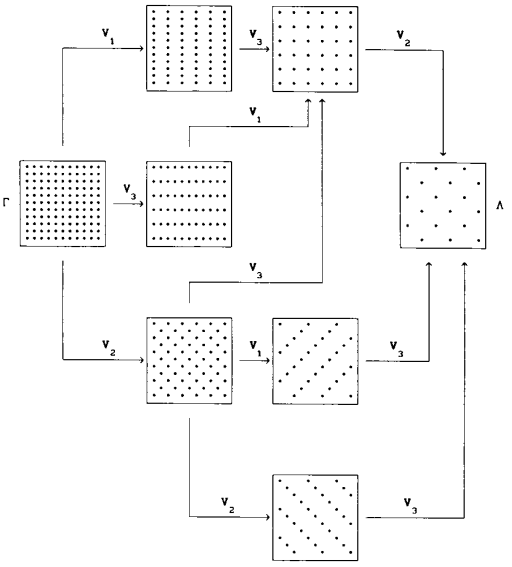

Fig. 1. The dlc on $\mathscr{A} = (2, 2, 2)$ from Γ to Λ relative to (10).

C. Multidimensional Sampling Structure Conversion

Consider M-dimensional lattices $\Lambda_1 = \mathrm{LAT}(A)$ and $\Lambda_2 = \mathrm{LAT}(C)$ and assume that $A^{-1}C \in \mathbb{Q}_M$ (so that $\Lambda_1 + \Lambda_2$ is a lattice, in force of Theorem 1). Let $B = AL^{-1} = CM^{-1}$ be a basis of $\Lambda_1 + \Lambda_2$. Signal x defined on Λ_1 can be converted into a signal defined on Λ_2, called y, by the cascade of an up-conversion, a linear filtering, and a down-conversion [2], [3].

The up-conversion (or up-sampling) between signal s defined on M-dimensional lattice Ψ_1 and signal w defined on M-dimensional lattice Ψ_2, with $\Psi_1 \subset \Psi_2$, is defined as

$$w(a) = \begin{cases} s(a), & a \in \Psi_1 \\ 0 & \text{otherwise} \end{cases} \qquad \text{with } a \in \Psi_2. \quad (12)$$

The down-conversion (or down-sampling) between signal u defined on M-dimensional lattice Γ_1 and signal v defined on M-dimensional lattice Γ_2, with $\Gamma_1 \supset \Gamma_2$, is defined as

$$v(a) = u(a) \qquad \text{with } a \in \Gamma_2. \quad (13)$$

If E is a basis of Ψ_1 and $F = EL^{-1}$ is a basis of Ψ_2, the up-converter will be denoted by the symbol of Fig. 2(a). If E is a basis of Γ_1 and $F = EM$ is a basis of Γ_2, the down-converter will be denoted by the symbol of Fig. 2(b).

The Fourier transform of a signal x defined on the M-dimensional lattice $\Lambda = \mathrm{LAT}(A)$ is defined as [2]

$$X(f) = \sum_{a \in \Lambda} x(a) \exp(-j2\pi f^T a), \qquad f \in \mathbb{R}^M \quad (14)$$

The Fourier transform $X(f)$ is periodic according to rule

$$X(f + b) = X(f), \qquad b \in \Lambda^* \quad (15)$$

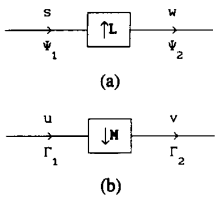

Fig. 2. (a) Up-converter; (b) down-converter.

therefore $X(f)$ is completely defined from its values on any fundamental cell $\mathscr{P}$ of Λ^*.

It is well known [2] that the Fourier transforms of the up-converter input and output are related as

$$W(f) = S(f) \tag{16}$$

and those of the down-converter input and output as

$$V(f) = \frac{1}{(\Gamma_1:\Gamma_2)} \sum_{c \in \Gamma_2^* \cap \mathscr{P}_1} U(f + c) \tag{17}$$

where $\mathscr{P}_1$ is a fundamental cell of Γ_1^*.

Fig. 3 shows the sampling structure conversion scheme between Λ_1 and Λ_2. The intermediate block of Fig. 3 represents a linear filter of impulse response $\boldsymbol{h}$ defined on $\Lambda_1 + \Lambda_2$. If $\mathscr{P}$ is a fundamental cell of $(\Lambda_1 + \Lambda_2)^* = \Lambda_1^* \cap \Lambda_2^*$, $\mathscr{P}_1$ a fundamental cell of Λ_1^* such that $\mathscr{P}_1 \subset \mathscr{P}$, and $\mathscr{P}_2$ a fundamental cell of Λ_2^* such that $\mathscr{P}_2 \subset \mathscr{P}$, there will be no aliasing (and hence perfect reconstruction within $\mathscr{P}_1 \cap \mathscr{P}_2$) if the Fourier transform of h is

$$H(f) = \begin{cases} (\Lambda_1 + \Lambda_2):\Lambda_2, & f \in \mathscr{P}_1 \cap \mathscr{P}_2 \\ 0, & \text{otherwise} \end{cases} \tag{18}$$

with $f \in \mathscr{P}$.

The choice of cells $\mathscr{P}_1$ and $\mathscr{P}_2$ is critical for the overall system performance, since it controls the system perfect reconstruction region. In principle, it is appropriate to choose $\mathscr{P}_1$ and $\mathscr{P}_2$ such that $\mathscr{P}_1 \cap \mathscr{P}_2$ covers the greatest possible portion of the hypervolumes of $\mathscr{P}_1$ and $\mathscr{P}_2$. Fig. 4(a) shows three possible choices of $\mathscr{P}_1$ and $\mathscr{P}_2$, relative to lattices

$$\Lambda_1^* = \mathrm{LAT}\begin{pmatrix} 4 & 0 \\ 0 & 4 \end{pmatrix} \quad \text{and} \quad \Lambda_2^* = \mathrm{LAT}\begin{pmatrix} 6 & 3 \\ 0 & 3 \end{pmatrix}.$$

Cell $\mathscr{P}_1$ is the solid-line square. The dashed rectangles and the dashed diamond of Fig. 4(a) are three possible choices of $\mathscr{P}_2$. Clearly, the diamond-shaped $\mathscr{P}_2$ gives the maximum hypervolume $\mathscr{P}_1 \cap \mathscr{P}_2$.

The maximization of the intersection's hypervolume may not be the only criterion worth adopting for the choice of $\mathscr{P}_1$ and $\mathscr{P}_2$. For instance, Fig. 4(b) shows three possible choices of $\mathscr{P}_1 \cap \mathscr{P}_2$, relative to lattices

$$\Lambda_1^* = \mathrm{LAT}\begin{pmatrix} 4 & 0 \\ 0 & 4 \end{pmatrix} \quad \text{and} \quad \Lambda_2^* = \mathrm{LAT}\begin{pmatrix} 4 & 2 \\ 0 & 3 \end{pmatrix}.$$

Cell $\mathscr{P}_1$ is the solid-line square. The dashed rectangle and the dashed hexagon are two possible choices of $\mathscr{P}_2$.

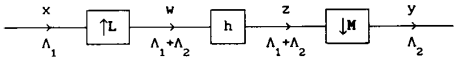

Fig. 3. Sampling structure conversion scheme.

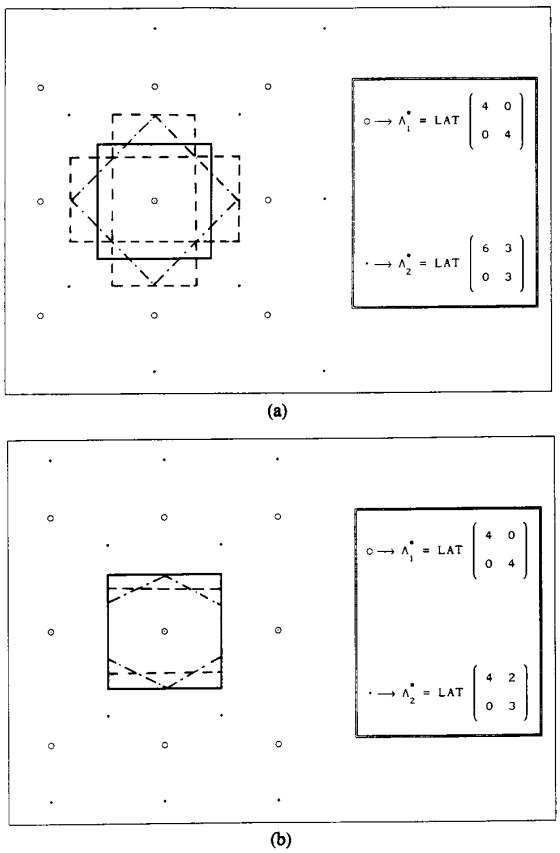

Fig. 4. Possible perfect reconstruction regions.

Clearly, the hypervolume of the intersection between the dashed rectangle of $\mathscr{P}_1$ is equal to the hypervolume of the intersection between the hexagon and $\mathscr{P}_1$. However, the latter choice of $\mathscr{P}_2$ may be more appropriate than the former, since it gives a better conservation of the energy along the two axes. Such a feature is visually very important [14]. Choices of $\mathscr{P}_1$ and $\mathscr{P}_2$ of this type are reported, for instance, in [16]. (The characterization of the convex fundamental cells of an M-dimensional lattice can be found in [15]).

The scheme of Fig. 3 is effective if the value $(\Lambda_1 + \Lambda_2:\Lambda_2)$ is not too large. For instance, the conversion from CCIR System I standard 525/2:1/60 to CCIR System M standard 625/2:1/50, considered in Subsection II-A and corresponding to $(\Lambda_1 + \Lambda_2:\Lambda_1) = 250$, can be more appropriately approached by techniques of the type proposed in [9].

The sampling structure conversion scheme (see Fig. 3) does not need the down-converter when $\Lambda_1 \subset \Lambda_2$, and it

does not need the up-converter when $\Lambda_1 \supset \Lambda_2$. In any case, though, the presence of the intermediate linear filter is necessary. The realization of such a filter requires the determination of $\Lambda_1 + \Lambda_2$ (achievable by the results of Subsection II-A) and the choice of $\mathscr{P}_1$ and $\mathscr{P}_2$ (by considerations of the type just exemplified). An efficient implementation of the scheme of Fig. 3 is considered in [11]; the next section discussed the effectiveness of the multistage realization of M-dimensional sampling structure conversion.

III. Multistage M-Dimensional Sampling Structure Conversion

The advantages of multistage implementation of 1-D FIR sampling rate converters are well known [1]. The efficiences of such structures are essentially due to the relationships between transition bandwidth (normalized with respect to the sampling frequency) and filter order for 1-D FIR filters. Given passband and stopband errors, the smaller the normalized transition bandwidth, the higher (typically) the order of the FIR filter achieving it. It turns out that performing the up-sampling (or the down-sampling) in several stages requires filters with larger (normalized) transition regions than a single-stage up-sampler, with remarkable overall performance gains.

The techniques originally proposed for designing IFIR filters [17], [18], are very effective also for designing the filters belonging to each stage, owing to the equivalence between multistage sampling rate converters and IFIR structures.

Similar concepts can be extended to the M-D case, as suggested in [19] and [12]. The motivation of the advantages of the multistage approach to M-D sampling structure conversion, along the lines of the theory developed for the 1-D case, is considerably complicated by the fact that, in the M-D case, transition bands are M-D regions (possibly irregular) and not simple intervals, as in the 1-D case. Although quantitative relationships between the orders of M-D FIR filters and their transition regions, for given passband and stopband errors, are not known, the conjecture that such orders increase as the transition regions' relative widths decrease is supported by considerable experimental evidence. The performance gains actually achievable by multistage sampling structure conversion schemes versus direct implementation confirm such a hypothesis.

In order to describe the multistage implementation of the sampling structure conversion procedure of Fig. 3, let us, for simplicity, focus on case $\Lambda_1 \subset \Lambda_2$. In such a circumstance, the system is formed only by the up-sampler and the linear filter.

Consider an ordered integer decomposition $\mathscr{A} = (\alpha_1, \alpha_2, \cdots, \alpha_p)$ of $(\Lambda_2 : \Lambda_1)$ and an ascending lattice chain $(\Phi_1, \Phi_2, \cdots, \Phi_{p-1})$ on $\mathscr{A}$ from Λ_1 to Λ_2 [see (11)]. For notational convenience let us denote $\Lambda_1 = \Phi_0$ and $\Lambda_2 = \Phi_p$. The sampling structure conversion from Λ_1 to Λ_2 can be performed by p subsystems, each one formed by an up-converter from Φ_i to Φ_{i+1}, $(i = 0, 1, \cdots, p-1)$ and a

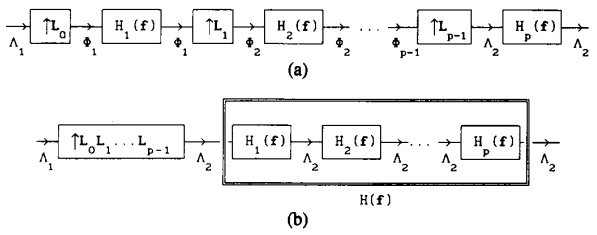

Fig. 5. (a) Multistage sampling structure conversion scheme; (b) equivalent system.

suitable linear filter $H_{i+1}(f)$, as shown in Fig. 5(a). If $\boldsymbol{P}$ is a basis of Λ_2 and $(\boldsymbol{L}_0, \boldsymbol{L}_1, \cdots, \boldsymbol{L}_{p-1})$ are matrixes as described in Subsection II-A, then $\Phi_i = \mathrm{LAT}(\boldsymbol{P}\boldsymbol{L}_{p-1} \cdots \boldsymbol{L}_i)$. By means of the multidimensional noble identity [20], [12], the scheme of Fig. 5(a) can be shown to be equivalent to that of Fig. 5(b). It is important to note that each transfer function $H_i(f)$ of Fig. 5(b) is periodic on Φ_i^*, while the corresponding impulse response is defined on Λ_2. (The description of the system of Fig. 5(b) in terms of M-D z-transform [20] would make apparent such a fact).

If the transfer function $H(f) = H_1(f)H_2(f) \cdots H_p(f)$ of the system of Fig. 5(b) is defined as in (18), then the system of Fig. 5(b), and its equivalent in Fig. 5(a), give perfect reconstruction in $\mathscr{P}_1 \cap \mathscr{P}_2$. The generalization of the scheme of Fig. 5 to the case of generic Λ_1 and Λ_2 is straightforward.

The advantages of the multistage scheme depend on the choice of factorization $\mathscr{A}$ (similarly to the 1-D case) and of the specific alc on $\mathscr{A}$ from Λ_1 to Λ_2, if there is more than just one. It is worth noting that the latter point does not have a counterpart in the 1-D case.

A. Useful Transfer Function Characteristics

The performance of a sampling structure converter operating in video signals may be enhanced by the following characteristics of the system transfer function.

As cleverly pointed out in [21], the avoidance of artifacts in flat areas due to aliasing requires that $H(f)$ of Fig. 5(b) satisfies to

$$H(f) = 0, \qquad f \in \Lambda_1^*, \qquad f \notin (\Lambda_1 + \Lambda_2)^*. \quad (19)$$

In the sampling structure conversion of video signals the use of (19) is mandatory.

In the 1-D case [1], [22], sampling rate conversion by means of M-band subfilters with impulse responses having zeroes on the intersections between the input and output domains of each stage (except at the origin) is computationally efficient and, in the up-sampling case, it preserves the input signal samples at the output. Such filter characteristics are typically referred to as Nyquist conditions.

The reasons supporting Nyquist filters in the 1-D case apply also to the M-D case [34]. If $h_i(\boldsymbol{a})$ denotes the impulse response of the subsystem with transfer function

$H_i(f)$ in Fig. 5(a), the filter satisfies to the Nyquist condition if

$$h_i(\boldsymbol{a}) = \begin{cases} 1, & \boldsymbol{a} = 0 \\ 0, & \boldsymbol{a} \in \Phi_{i-1} - \{0\} \end{cases} \tag{20}$$

with $\boldsymbol{a} \in \Phi_i$.
Condition (20) in the frequency domain becomes

$$\sum_{\boldsymbol{c} \in (\Phi_{i-1}^* \cap \mathscr{P}_i)} H_i(\boldsymbol{f} + \boldsymbol{c}) = (\Phi_i : \Phi_{i-1}) = \alpha_i \tag{21}$$

where $\mathscr{P}_i$ is a fundamental cell of Φ_I^*.

IV. A Study Case: Video Format Conversion

As an example of a practical situation where the multistage implementation presented in the previous section may be profitably applied, consider the format conversion from aspect ratio 4/3 to aspect ratio 16/9 of a 2:1 interlaced television signal. The parameters entering the problem can be seen from Fig. 6. In Fig. 6, both formats are drawn with the same picture width in order to explicitly account for the fact that the line periods are the same for both aspect ratios. In the case of aspect ratio 4/3, the relationship between picture height P_h and picture width P_w is $P_h = \frac{3}{4}P_w$, and in the case of aspect ratio 16/9 it is $\bar{P}_h = \frac{9}{16}P_w$. As the number of lines N is the same in both cases, the interline distances $\bar{d}_y$ concerning 16/9 aspect ratio, and d_y concerning 4/3 aspect ratio are related as

$$\bar{d}_y = \frac{\bar{P}_h}{N} = \frac{3}{4}\frac{P_h}{N} = \frac{3}{4}d_y. \tag{22}$$

A possibility of converting aspect ratio 4/3 into 16/9 is that of mapping $N \cdot 3/4$ lines of the input images, with 4/3 aspect ratio, into N lines of the output images, with 16/9 aspect ratio. The implications of such a format conversion solution are considered in detail.

Fig. 7(a) shows the verticotemporal lattices associated to the two aspect ratios; T_f denotes the field period and interlace 2:1 is assumed.

A basis of lattice Λ_1, relative to the verticotemporal section of aspect ratio 4/3, is

$$\boldsymbol{A} = \begin{pmatrix} 2T_f & T_f \\ 0 & d_y \end{pmatrix},$$

while a basis of lattice Λ_2, relative to the verticotemporal section of aspect ratio 16/9, is

$$\boldsymbol{C} = \begin{pmatrix} 2T_f & T_f \\ 0 & \frac{3}{4}d_y \end{pmatrix}.$$

By Theorem 1, since

$$\boldsymbol{A}^{-1}\boldsymbol{C} = \begin{pmatrix} 1 & \frac{1}{8} \\ 0 & \frac{3}{4} \end{pmatrix}$$

belongs to $\mathbb{Q}_2$, lattice $\Lambda_1 + \Lambda_2$ exists. Also, by Corollary 1, since $\det(\boldsymbol{A}^{-1}\boldsymbol{C}) = 8$ and $\det(\boldsymbol{A}^{-1}\boldsymbol{C}) = \frac{3}{4}$, it is $(\Lambda_1 + \Lambda_2 : \Lambda_1) = 8$. A basis of $\Lambda_1 + \Lambda_2$ can be found by Theorem 1 and the procedure described in the Appendix.

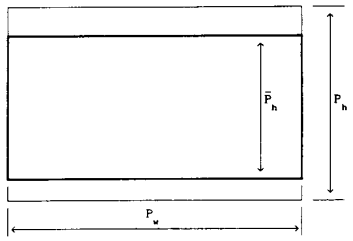

Fig. 6. Format parameters relative to 4/3 (thin line) and 16/9 (bold line) aspect ratios.

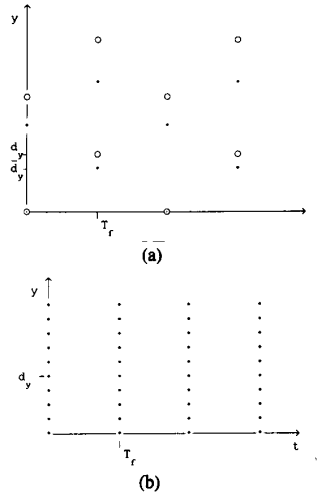

Fig. 7. (a) Lattices corresponding to the verticotemporal intersection of the scanning rasters for 4/3 aspect ratio (Λ_1, circles) and 16/9 aspect ratio (Λ_2, dots); (b) lattice $\Lambda_1 + \Lambda_2$.

Unimodular matrixes

$$\boldsymbol{U} = \begin{pmatrix} 1 & 0 \\ 6 & -1 \end{pmatrix}$$

and

$$\boldsymbol{V} = \begin{pmatrix} 0 & 1 \\ 1 & -8 \end{pmatrix}$$

are such that

$$\boldsymbol{D} = \boldsymbol{U}(\boldsymbol{A}^{-1}\boldsymbol{C})\boldsymbol{V} = \begin{pmatrix} \frac{1}{8} & 0 \\ 0 & 6 \end{pmatrix}$$

is in Smith–McMillan normal form. Hence, by Result A.5, $(\boldsymbol{H}, \boldsymbol{K})$ with

$$\boldsymbol{H} = \begin{pmatrix} 8 & 0 \\ 0 & 1 \end{pmatrix} \cdot \boldsymbol{U} = \begin{pmatrix} 8 & 0 \\ 6 & -1 \end{pmatrix},$$

$$\boldsymbol{K} = \begin{pmatrix} 1 & 0 \\ 0 & 6 \end{pmatrix} \cdot \boldsymbol{V}^{-1} = \begin{pmatrix} 8 & 1 \\ 6 & 0 \end{pmatrix}$$

is a left-coprime factorization of $\boldsymbol{A}^{-1}\boldsymbol{C}$.

Then, a basis of $\Lambda_1 + \Lambda_2$ is

$$\boldsymbol{B} = \boldsymbol{A}\boldsymbol{H}^{-1} = \begin{pmatrix} T_f & -T_f \\ \frac{3}{4}d_y & -d_y \end{pmatrix}$$

[see Fig. 7(b)] where, according to CCIR System M standard 625/2:1/50, $T_f = 1/50$ s and $d_y = P_h/N$ with $N = 625$.

Three possible bases of the dual lattices are

$$\mathbf{A}^{-T} = \begin{pmatrix} \frac{1}{2T_f} & 0 \\ \frac{-1}{2d_y} & \frac{1}{d_y} \end{pmatrix}, \quad \mathbf{C}^{-T} = \begin{pmatrix} \frac{1}{2T_f} & 0 \\ \frac{-2}{3d_y} & \frac{4}{3d_y} \end{pmatrix},$$

$$\mathbf{B}^{-T} = \begin{pmatrix} \frac{4}{T_f} & \frac{3}{T_f} \\ \frac{-4}{d_y} & \frac{-4}{d_y} \end{pmatrix}$$

where $1/T_f = 50$ Hz and $1/d_y = 625$ c/Ph (see Fig. 8).

Completely similar considerations apply to the case of CCIR System I 525/2:1/60.

The sampling structure conversion from Λ_1 to $\Lambda_1 + \Lambda_2$, according to the scheme of Fig. 3, requires seven new lines for each input line. The conversion from $\Lambda_1 + \Lambda_2$ to Λ_2 requires keeping one out of six lines, of the signal defined on $\Lambda_1 + \Lambda_2$. Such an operation can be performed either by the single-step scheme of Fig. 3 or by a multistage scheme of the type of Fig. 5(a) for the interpolation, possibly cascaded by a similar arrangement for the decimation.

Let us first consider the single-stage scheme of Fig. 3. As explained in Section 2, the passband of the ideal low-pass filter [see (18)] is given by the intersection of a fundamental cell of Λ_1^* with a fundamental cell of Λ_2^*. An effective choice for such a region is shown in Fig. 9(a). The passband is the diamond of Fig. 9(a). The filter stopband is the region of the fundamental cell of $(\Lambda_1 + \Lambda_2)^*$ complementary to the diamond. A realistic design mask for the filter of Fig. 9(a) is shown in Fig. 9(b), where the dotted region is the transition region (only the first quadrant is shown, as the filter has quandrantal symmetry).

As explained in Subsection III-A, it is important that the specs incorporate condition [see (19)]. Such conditions impose that the transfer function be exactly zero at the points marked by crosses in Fig. 9(b).

Zero-phase FIR filters with transfer functions optimal in the minimax sense, with respect to the mask of Fig. 9(b), were designed by linear programming [23]. (The effectiveness of linear programming in these applications is well known [24], [16].)

Fig. 10 (dotted line) shows the minimax errors (normalized to unity), corresponding to equal error weights in both passband and stopband, for filters of different $N_y \times N_t$ size. As $(N_t - 1)$ corresponds to the number of field memories (FIFO) required by the filter, the examined values were limited to N_t equal to 3, 5 and 7. Vertical length N_y, associated to the number $(N_y - 1)$ of line memories, was allowed to assume considerably higher values.

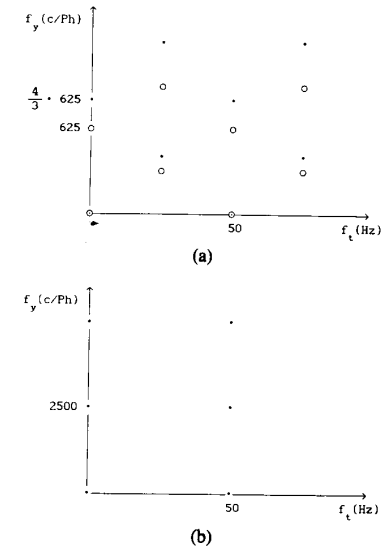

Fig. 8. (a) Lattice Λ_1^* (dots) and Λ_2^* (circles); (b) lattice $(\Lambda_1 + \Lambda_2)^*$.

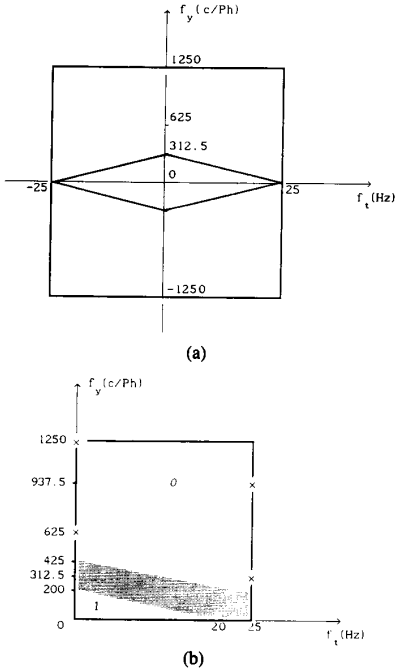

Fig. 9. Transfer function [see (18)]: (a) ideal mask; (b) actual design mask.

It is clear from Fig. 10 that, for given N_t values, the normalized minimax error tends to saturate as N_y increases. For instance, if $N_t = 3$, the normalized minimax error tends to saturate to approximately 0.11.

The multistage realization of the format conversion system can be performed in many ways as $(\Lambda_1 + \Lambda_2 : \Lambda_1) = 8$ and $(\Lambda_1 + \Lambda_2 : \Lambda_2) = 6$. The lattice chains for the interpolation and decimation steps are summarized by Table I. Fig. 11 sketches such possibilities, according to the conventions introduced for Fig. 1. Fig. 11(a) refers to the possible alc performing the up-conversion from Λ_1 to $\Lambda_1 + \Lambda_2$, and Fig. 11(b) to the possible dlc relative to the down-conversion from $\Lambda_1 + \Lambda_2$ to Λ_2.

An interesting choice is a indicated by the bold path of Fig. 11, considering a two-stage interpolation, where the first step converts the signal from standard 625/2:1/50 to standard 1250/1:1/50, the second step brings it to standard 2500/1:1/50, and a single-stage decimation brings it to $(\frac{3}{4} \cdot 625)/2:1/50$.

Fig. 12(a) shows the design specs of the first-stage interpolation filter $H_1(f_y, f_t)$ (the crosses represent the points where the transfer function is constrained to be zero). Fig. 12(b) shows the specs of the second-stage (1-D) interpolation filter $H_2(f_y)$. It is important to note that the vertical width of the transition region of Fig. 12(a), normalized to the "vertical" sampling frequency, doubles the corresponding quantity of Fig. 9(b). It is well known [25] that such a characteristic, in the 1-D case, allows the attainment of a given minimax error by halving the filter order. This type of trend is therefore expected also in the case of the filter of Fig. 12(a), and it is experimentally confirmed.

Fig. 10 (bold line) shows the normalized minimax errors of the FIR filters $H_1(f_y, f_t)$ approximating the specs of Fig. 12(a) for different $N_y' \times N_t'$ sizes. The minimax errors for given N_t' values, and for the same vertical order, are smaller than the corresponding errors of the single-stage filter.

The second-stage interpolation filter (which operates only on the lines) has a large transition band. As its transfer function has to be zero at $f_y = 1250$ c/Ph, a raised cosine qualifies as an effective choice for such a filter. In this case, the second-stage filter size has $N_t'' = 1$ (no field memory) and $N_y'' = 3$.

The global performance of the two-stage interpolator is given by the product of $H_1(f_y, f_t)$ with $H_2(f_y)$. As hinted by Fig. 12(c), the global performance approximates the design specs of Fig. 9(b).

Let δ_p' and δ_s' denote the passband and stopband errors of $H_1(f_y, f_t)$, and δ_p'' and δ_s'' the corresponding quantities of $H_2(f_y)$. The global passband error is therefore less than or equal to $\delta_p' + \delta_p''$, and the global stopband error is less than or equal to $\max\{\delta_s', \delta_s''\}$. It is clear that in the intersection between the stopbands of the two systems, the stopband error is less than or equal to $\delta_s' \delta_s''$.

It is rather instructive to compare the single-stage interpolation scheme with the two-stage scheme. Let the minimax error of the single-stage interpolation be $\delta_p = \delta_s$.

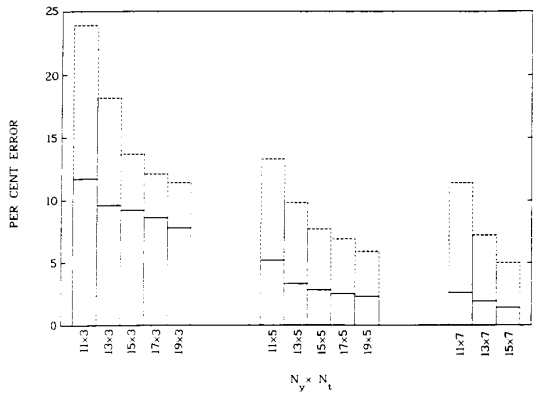

Fig. 10. Minimax errors of FIR filters designed according to the specs of Fig. 9(b) (dotted line) and Fig. 12(a) (solid line).

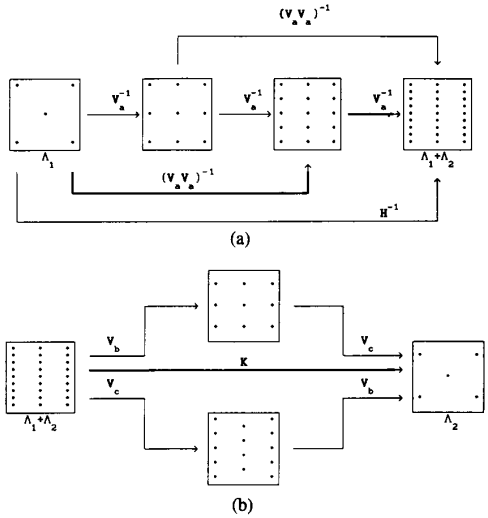

Fig. 11. Lattice chains corresponding to Table I: (a) Λ_1 to $\Lambda_1 + \Lambda_2$ conversion; (b) $\Lambda_1 + \Lambda_2$ to Λ_2 conversion.

TABLE I
POSSIBLE LATTICE CHAINS FOR 4 / 3 TO 16 / 9 FORMAT CONVERSION

$\Lambda_1 = \mathrm{LAT}(\boldsymbol{BH}) \rightarrow \Lambda_1 + \Lambda_2 = \mathrm{LAT}(\boldsymbol{B})$	
$\mathscr{A}$	alc
(2, 2, 2)	$(\mathrm{LAT}(\boldsymbol{BV}_a\boldsymbol{V}_a), \mathrm{LAT}(\boldsymbol{BV}_a))$
(2, 4)	$(\mathrm{LAT}(\boldsymbol{BV}_a\boldsymbol{V}_a))$
(4, 2)	$(\mathrm{LAT}(\boldsymbol{BV}_a))$
$\Lambda_1 + \Lambda_2 = \mathrm{LAT}(\boldsymbol{B}) \rightarrow \Lambda_2 = \mathrm{LAT}(\boldsymbol{BK})$	
$\mathscr{A}$	dlc
(2, 3)	$(\mathrm{LAT}(\boldsymbol{BV}_b))$
(3, 2)	$(\mathrm{LAT}(\boldsymbol{BV}_c))$

$$\boldsymbol{H} = \begin{pmatrix} 8 & 0 \\ 6 & -1 \end{pmatrix} \quad \boldsymbol{K} = \begin{pmatrix} 8 & 1 \\ 6 & 0 \end{pmatrix}$$

$$\boldsymbol{V}_a = \begin{pmatrix} 2 & 0 \\ 0 & 1 \end{pmatrix} \quad \boldsymbol{V}_b = \begin{pmatrix} 1 & 0 \\ 0 & 3 \end{pmatrix} \quad \boldsymbol{V}_c = \begin{pmatrix} 1 & 0 \\ 0 & 2 \end{pmatrix}$$

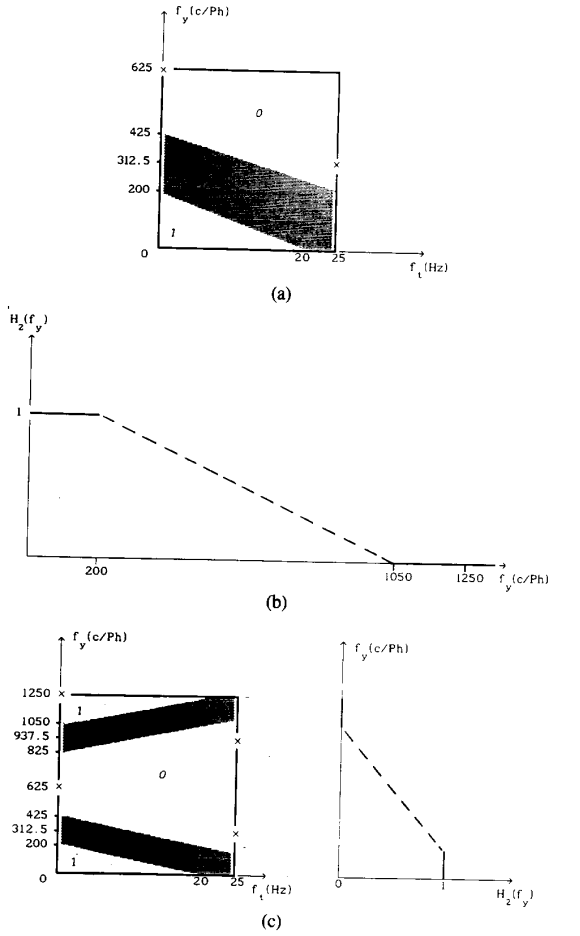

Fig. 12. Multistage interpolation: (a) first filter specs; (b) second filter specs; (c) global specs (sketch).

Equal performance by the two schemes, at a given global minimax error, requires that $\delta_p = \delta_p' + \delta_p''$ and $\delta_s = \delta_s'$. It is also convenient to impose $\delta_s' = \delta_s''$. As $\delta_p'' = 0.032$ and $\delta_s'' = 0.064$ (from the raised cosine), the first-stage interpolator has to have $\delta_s' = 0.064$ and $\delta_p' \leq \delta_p - 0.032 = 0.032$ (as $\delta_p = \delta_s$). From Fig. 10 it can be seen, for instance, that the performance of the single-stage interpolator of size 17×5 is matched by the two-stage interpolator with $H_1(f_y, f_t)$ of size 11×5, followed by the raised cosine. Hence the two-stage interpolator scheme is advantageous with respect to the number of line memories.

It is important to observe that in the considered example, the multistage decomposition is active *only* along the vertical direction. Such a fact is likely to be responsible for the mild overall performance gains of the two-stage scheme with respect to the single-stage scheme. It is straightforward that in situations where the sampling rate changes in both directions, the possible advantages are closer to those of the 1-D case. (As a simple example, consider a situation where separable filters can be employed).

The memory savings obtainable by multistage schemes are accompanied by computational savings only in cases of pure up-conversion or pure down-conversion. When both conversion types occur, as in the considered example, this is not necessarily true. For instance, as pointed out by a Referee, in the format conversion case single-stage implementation allows one to compute only one out of six samples of the intermediate lattice, $\Lambda_1 + \Lambda_2$. A similar possibility in the two-stage approach is available only in the second stage.

However, one should observe that the number of allotted field memories was only $N_t - 1 = 4$. Also, in the 1-D case multistage implementation is hardly of any use with five coefficients filters. Conceivably, higher N_t values—closer to those for which multistage implementation leads to order savings in the 1-D case—in addition to line memories savings may also give field memory savings.

It should be observed that, also in the case of single-direction sampling rate changes like the considered format-conversion example, multistage schemes present advantages not merely expressable in terms of minimax errors but quite significant in practice. Such aspects are related to the overall regularity, or smoothness, of the system transfer function, to the system ringing behavior, and to the visual rendition.

Fig. 13 shows the transfer function of a 17×5 single-stage interpolator approximating the specs of Fig. 9(b)[1]. Fig. 14 shows a 11×5 first-stage interpolator $H_1(f_y, f_t)$, designed according to the specs of Fig. 12(a) (shown in the fundamental cell of the dual of the intermediate lattice, related to standard 1250/1:1/50). Fig. 15 shows the transfer function of the overall two-stage interpolator $H_1(f_y, f_t) \cdot H_2(f_y)$ with $N_y' = 11$, $N_t' = 5$, and $N_y'' = 3$. The regularity of the latter transfer function is superior to that of the transfer function of Fig. 13.

M-D FIR filters optimal in the minimax sense, not differently than the 1-D FIR filters, have a number of equal error ripples increasing with their orders [26]. Therefore, the FIR filters in the saturation region of Fig. 10 have error values rather close but transfer functions increasingly oscillating as their orders increase. Such oscillations can be seen in the single-stage filter of Fig. 13. The oscillations of the two-stage filter are essentially due to filter $H_1(f_y, f_t)$. Such a filter corresponds to transition region requirements [Fig. 12(a)] more relaxed than those relative to the single-stage filter [Fig. 9(b)]. Therefore such specs are very likely to be satisfied by $H_1(f_y, f_t)$ filters not quite in the saturation region and with a limited number of transfer function oscillations, i.e., with a more regular transfer function behavior. The perceptual relevance of transfer function regularity is well acknowledged in the field [27].

The two-stage implementation also presents advantages over the single-stage filter with respect to system ringing. Fig. 16 compares three sections of the step responses of

[1] The coefficients of the filters of this paper are available upon request.

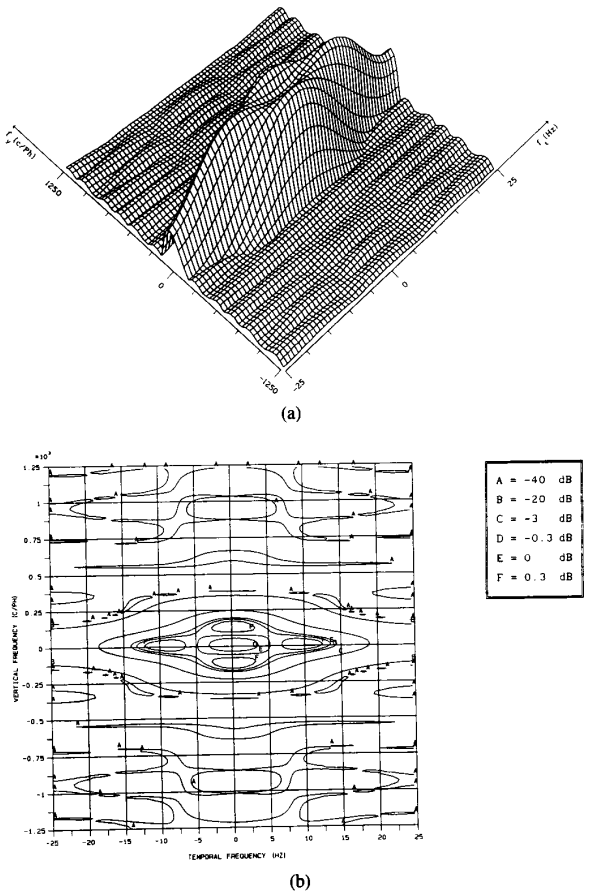

Fig. 13. Magnitude of the transfer function of the single-stage interpolation filter: (a) perspective plot; (b) contour plot.

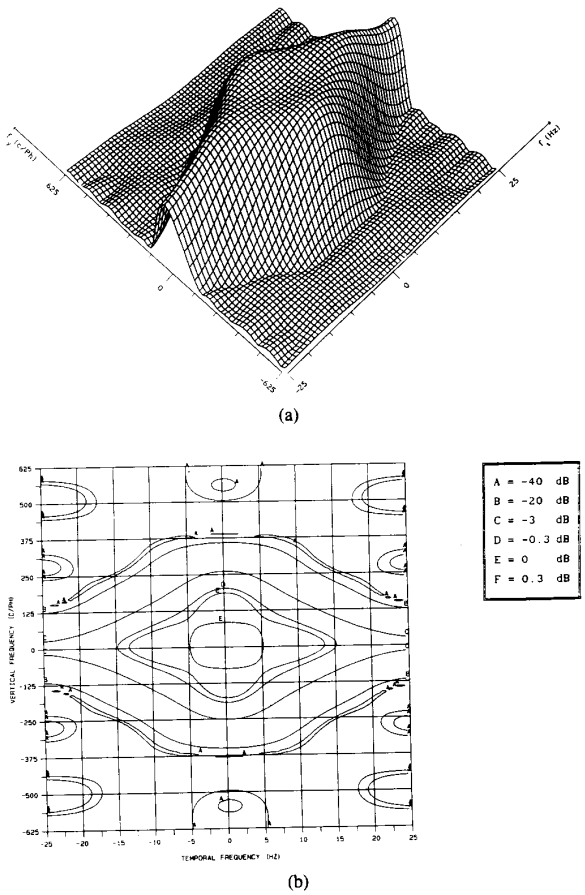

Fig. 14. Magnitude of the transfer function of the first stage interpolator filter: (a) perspective plot; (b) contour plot.

the single-stage filter (dotted line) with those of the double-stage filter (solid line). The considered step responses correspond to a vertical step [Fig. 16(a)]:

$$s_V(n_y, n_t) = \begin{cases} 1, & n_y \geq 0 \\ 0, & \text{otherwise} \end{cases} \tag{23}$$

a temporal step [Fig. 16(b)]

$$s_T(n_y, n_t) = \begin{cases} 1, & n_t \geq 0 \\ 0, & \text{otherwise} \end{cases} \tag{24}$$

and a diagonal step [Fig. 16(c)]

$$s_D(n_y, n_t) = \begin{cases} 1, & n_y + n_t \geq 0 \\ 0, & \text{otherwise} \end{cases} \tag{25}$$

The vertical step response accounts for the vertical ringing relative to horizontal (still) edges, and the temporal step response for the temporal ringing, or flashing, relative to sudden appearances of objects into the scene. The verticotemporal, or diagonal, step response accounts for the ringing relative to horizontal edges moving along the vertical direction. The usefulness of considering different step responses has recently been pointed out [28].

From Fig. 16 it is clear that the undershoot and the overshoot of the two-stage system are smaller than those of the single-stage system for each type of step response. Such a fact can be justified in light of the relationships between transition bandwidth and step response. It is well known that in the case of 1-D filters, the smaller the transition bandwidth the greater the step response's undershoot and overshoot. A similar behavior is expected with M-dimensional systems.

The ringing behavior of the single-stage filter is related to the normalized transition region of Fig. 9(b). The ringing behavior of the two-stage system is due to the normalized transition region of Fig. 12(a) for the first stage [which is much larger than that of Fig. 9(b)] and to the raised cosine for the second stage. The raised cosine (like any system with nonnegative impulse response) does not increase the overshoot, or the undershoot, of a system with which it is cascaded, but it can only increase the overall raise and settling times. Therefore, the ringing of the two-stage system is inferior to that of the single-stage system.

The visual rendition of the two-stage interpolator is indicated by Fig. 17, showing frame 37 of the television

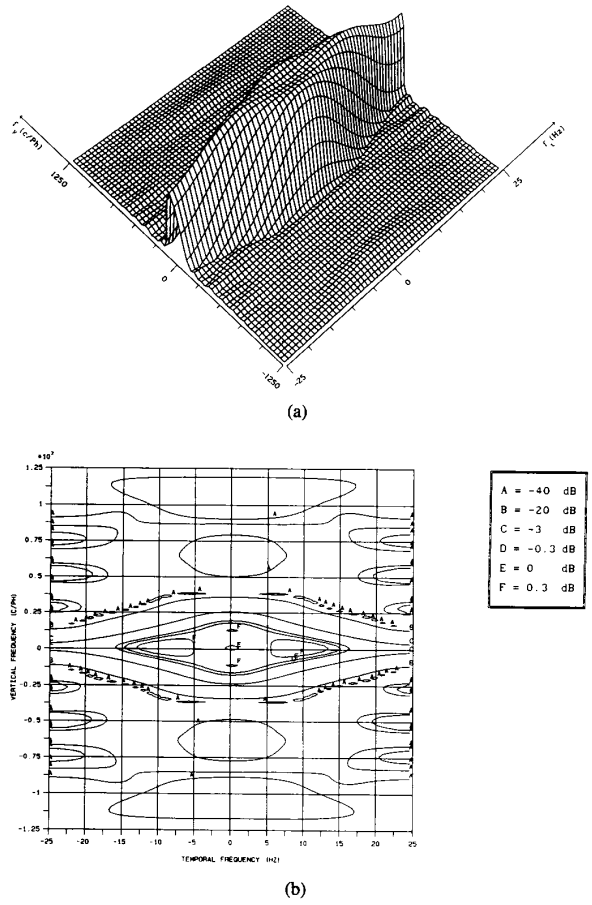

Fig. 15. Magnitude of the transfer function of the two-stage interpolator filter: (a) perspective plot; (b) contour plot.

sequence Girls. (The elongated shapes of the scene's objects occur because the 16/9 image is displayed on a conventional 4/3 monitor). With time-varying sequences, the transfer function regularity and the ringing behavior of the two-stage system manifest a superior visual rendition with respect to the single-stage system. Unfortunately, such a charcteristic cannot be well appreciated by photographs.

The use of single-stage and multistage format converters satisfying the Nyquist constraint (20) has also been examined. The desired transfer functions can be easily obtained by the adopted transfer function design tool of [23] (see also [29], [30]). The use of the Nyquist constraints presents computational advantages. For instance, in the case of the considered single-stage system with impulse response of size 17×5, 12 coefficients out of 85 are forced to be zero; in the case of the 11×5 filter of the first stage of the two-stage system, 12 coefficients out of 55 are forced to zero.

Clearly, the reduction of the coefficients number corresponds to the reduction of the system degrees of freedom. The minimax errors of the transfer functions satisfying to

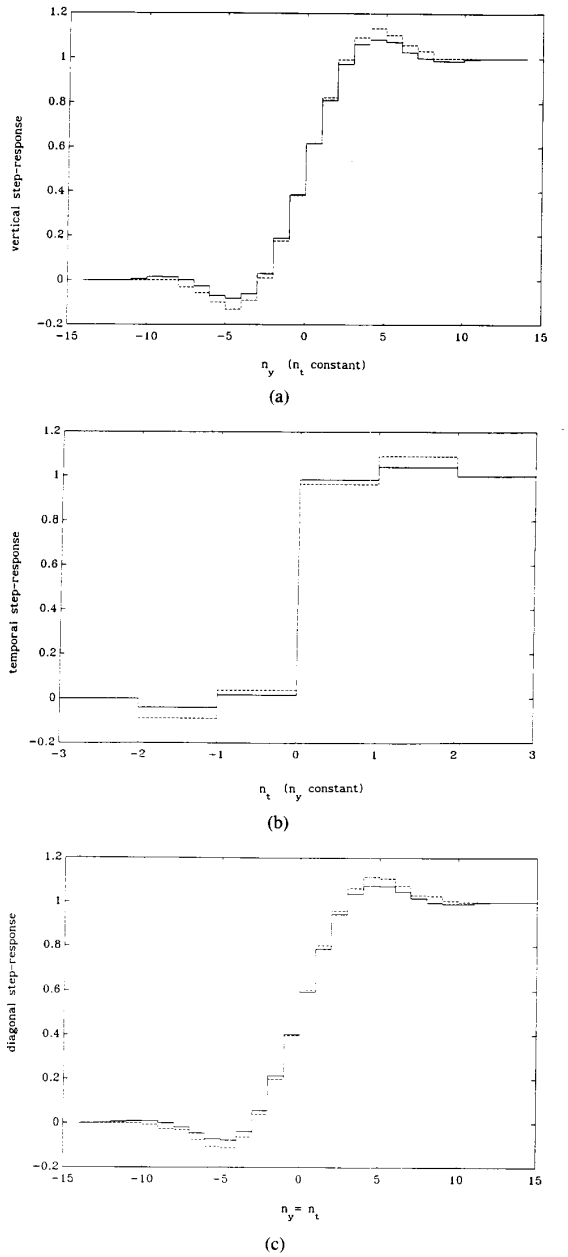

Fig. 16. Step responses of the single-stage (dotted line) and the two-stage (solid line) filters: (a) vertical step response; (b) temporal step response; (c) diagonal or verticotemporal step response.

the Nyquist constraints are expected to be greater than those of the unconstrained transfer functions. Figs. 18, 19, and 20 show the counterparts of the transfer functions of Figs. 13, 14, and 15, designed under the Nyquist constraints. The overall transfer function degradation is noticeable, and the corresponding perceptual rendition is not of the quality of the unconstrained systems. In this case, the computational load reduction comes at a performance price.

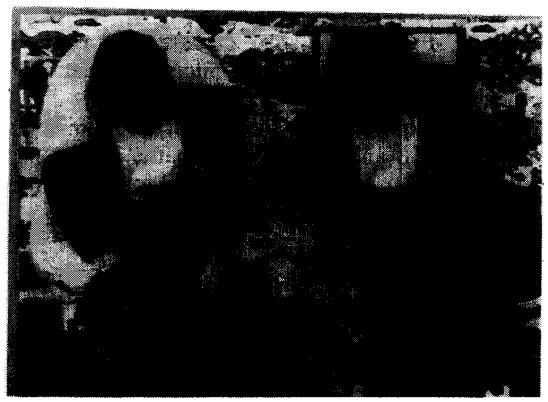

Fig. 17. Frame 37 of television sequence Girls (courtesy of Centro Ricerche RAI, Torino) converted from format 4/3 to 16/9 by the system based on the two-stage interpolator.

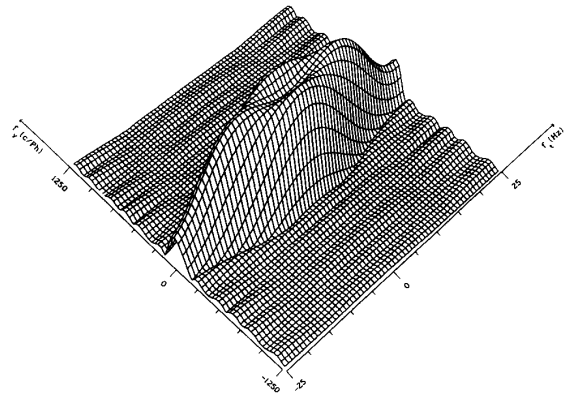

(a)

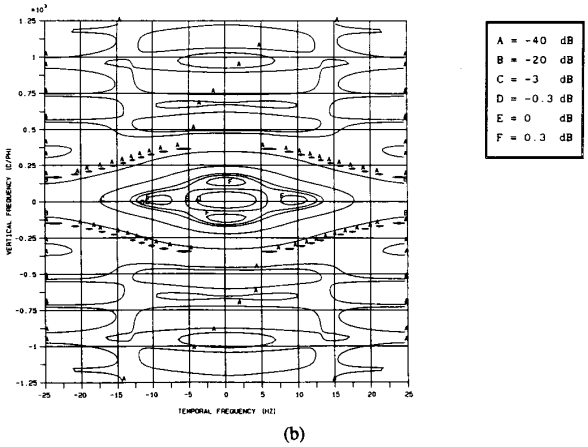

(b)

Fig. 18. Magnitude of the transfer function of the single-stage interpolation filter with the Nyquist constraints incorporated: (a) perspective plot; (b) contour plot.

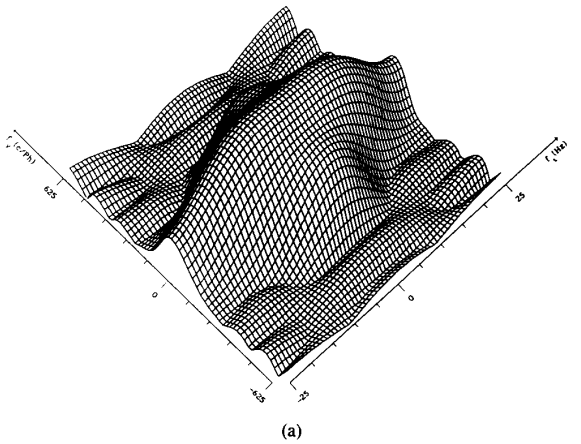

(a)

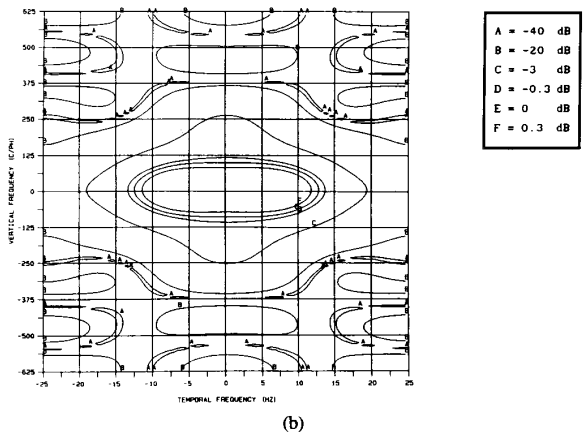

(b)

Fig. 19. Magnitude of the transfer function of the first-stage interpolator filter with the Nyquist constraint incorporated: (a) perspective plot; (b) contour plot.

V. Conclusion

This work extends multistage sampling structure conversion to the M-D case.

Two important aspects of the practical application of the sampling structure conversion scheme of Fig. 3 ([2], [3]), namely the determination of $\Lambda_1 + \Lambda_2$ and of the specs best suited to the linear filter, have been examined in depth.

Multistage implementation of M-D sampling structure conversion has been formally introduced and analyzed with respect to several points of view. The concepts have been applied to video format conversion. Even though the theoretical prediction of the system performance improvements attainable by multistage sampling structure conversion is not available, the considered examples have shown that multistage schemes are worth considering for video applications. This is probably the most interesting indication of the paper. It is also noticeable that, due to the complete equivalence between the idea of M-D multistage implementation and the idea of M-D IFIR filters [12],

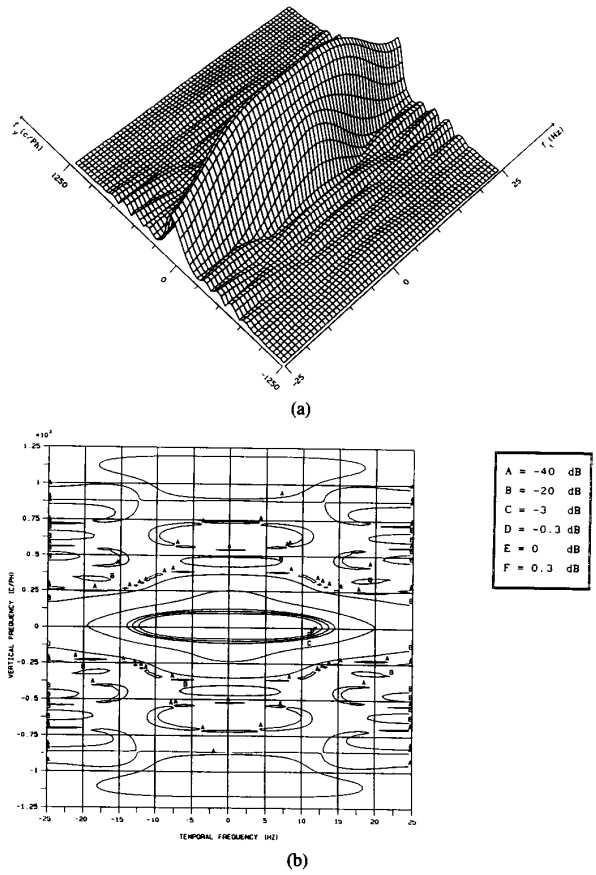

(a) (b)

Fig. 20. Magnitude of the transfer function of the two-stage interpolator filter with the Nyquist constraints incorporated: (a) perspective plot; (b) contour plot.

[19], the results presented in this work can be used in the context of M-D IFIR filters.

Further work is necessary for a deeper understanding of the mechanisms behind the performance improvements allowed by multistage schemes and for their most effective exploitation. An open issue, currently under study, is the individuation of the lattice decompositions associated with the multistage implementations of best overall performance.

Appendix

This Appendix presents a number of matrix theory results and notions used in various parts of the paper.

Let $\mathbb{Z}_M$, $\mathbb{Q}_M$, and $\mathbb{R}_M$ denote the rings of $M \times M$ matrixes with integer, rational, and real entries respectively.

Given integer l and m, if there is an integer n such that $l = mn$, then m is said to divide l (written $l|m$).

Given $a \in \mathbb{Q}$, $\mathrm{den}(a)$ denotes the least positive integer such that $(\mathrm{den}(a) \cdot a) \in \mathbb{Z}$. Given matrix $\boldsymbol{A} \in \mathbb{Q}_M$, $\mathrm{den}(\boldsymbol{A})$ will denote the least positive integer such that $(\mathrm{den}(\boldsymbol{A}) \cdot \boldsymbol{A}) \in \mathbb{Z}_M$, that is, $\mathrm{den}(\boldsymbol{A})$ is the least common multiple among $\{\mathrm{den}(a_{ij})\}$, where a_{ij} are the entries of $\boldsymbol{A}$.

Any full rank matrix $\boldsymbol{A} \in \mathbb{Z}_M$ such that $\boldsymbol{A}^{-1} \in \mathbb{Z}_M$ is called unimodular. It is easy to see that $\boldsymbol{A} \in \mathbb{Z}_M$ is unimodular if and only if $|\det(\boldsymbol{A})| = 1$.

Matrixes $\boldsymbol{A} \in \mathbb{Z}_M$ and $\boldsymbol{B} \in \mathbb{Z}_M$ are right-equivalent (left-equivalent) if there exists a unimodular matrix $\boldsymbol{V} \in \mathbb{Z}_M$ such that $\boldsymbol{B} = \boldsymbol{AV}$ ($\boldsymbol{B} = \boldsymbol{VA}$). Matrixes $\boldsymbol{A} \in \mathbb{Z}_M$ and $\boldsymbol{B} \in \mathbb{Z}_M$ are equivalent if there exist two unimodular matrixes $\boldsymbol{U} \in \mathbb{Z}_M$ and $\boldsymbol{V} \in \mathbb{Z}_M$ such that $\boldsymbol{B} = \boldsymbol{UAV}$.

Matrix $\boldsymbol{A} \in \mathbb{Z}_M$ is in Hermite normal form if

i) $\boldsymbol{A}$ is upper triangular

ii) $a_{ij} \geq 0$

iii) $a_{ij} < a_{ii}, \quad 1 \leq i < j \leq M, \quad$ if $a_{ii} \neq 0$

iiii) $a_{ij} = 0 \quad$ if $a_{ii} = 0$ (A.1)

where a_{ij} are the entries of $\boldsymbol{A}$.

Result A.1: Every full rank matrix of $\mathbb{Z}_M$ is right equivalent to one, and only one, Hermite normal form matrix. ■

Matrix $\boldsymbol{A} \in \mathbb{Z}_M$ is in Smith normal form if

i) $\boldsymbol{A} = \mathrm{diag}(a_1, a_2, \cdots, a_r, 0, \cdots, 0)$

ii) $a_i > 0, \quad 1 \leq i \leq r$

iii) $a_{i+1} | a_i, \quad 1 \leq i < r.$ (A.2)

Result A.2: Every matrix of $\mathbb{Z}_M$ is equivalent to one, and only one, Smith normal form matrix. ■

By means of Result A.2 it is easy to prove the following corollary:

Result A.3: Let $\boldsymbol{A}$ be a matrix of $\mathbb{Z}_M$ with $|\det(\boldsymbol{A})| = mn$, where m and n are positive integers. There exist matrixes $\boldsymbol{B}, \boldsymbol{C} \in \mathbb{Z}_M$ such that

i) $|\det(\boldsymbol{B})| = m, |\det(\boldsymbol{C})| = n$

ii) $\boldsymbol{A} = \boldsymbol{BC}$. ■ (A.3)

Matrix $\boldsymbol{A} \in \mathbb{Q}_M$ is in Smith–McMillan normal form if

i) $\mathbf{A} = \mathrm{diag}\left(\frac{a_1}{b_1}, \frac{a_2}{b_2}, \cdots, \frac{a_r}{b_r}, 0, \cdots, 0\right)$

with $a_i, b_i \in \mathbb{Z}$ coprime

ii) $a_{i+1} | a_i, \quad i = 1, \cdots, r-1$

iii) $b_i | b_{i+1}, \quad i = 1, \cdots, r-1.$ (A.4)

Without loss of generality, it can be assumed that $a_i > 0$, $b_i > 0$ for $1 \leq i \leq r$.

Result A.4: Given matrix $\boldsymbol{A} \in \mathbb{Q}_M$, there exist unimodular matrixes $\boldsymbol{U}$ and $\boldsymbol{V}$ of $\mathbb{Z}_M$ such that $\boldsymbol{S} = \boldsymbol{UAV}$ is in Smith–McMillan normal form, and such a reduction is unique. Furthermore, b_1 (the denominator of the $(1,1)$ entry of $\boldsymbol{S}$) is equal to $\mathrm{den}(\boldsymbol{A})$. ■

The proofs of the above results may be found in [8], [6], and [10]. An algorythm for finding unimodular matrixes $\boldsymbol{U},\boldsymbol{V}$ such that $\boldsymbol{UAV}$ is in Smith–McMillan normal form for a given $\boldsymbol{A} \in \mathbb{Q}_M$ may be based on the following concept [10]. Let $m = \mathrm{den}(\boldsymbol{A})$, then $m\boldsymbol{A} \in \mathbb{Z}_M$. If $\boldsymbol{U}$ and

V are unimodular matrixes of $\mathbb{Z}_M$ such that $U(mA)V$ is in Smith normal form, then $S = UAV$ is in Smith–McMillan normal form.

Given matrixes $A, D \in \mathbb{Z}_M$, D is a left divisor of A and A is a right multiple of D, if there exists a matrix $C \in \mathbb{Z}_M$ such that $A = DC$.

Given matrixes $A, B, D \in \mathbb{Z}_M$, D is a greatest common left divisor (gcld) of A and B if

i) **D** is a left divisor of both **A** and **B**

ii) **D** is a right multiple of every common

left divisor of **A** and **B**. (A.5)

Two matrixes A, B $\mathbb{Z}_M$ are left coprime if every gcld of A and B is unimodular.

The concept of common left divisor (or common right multiple) can be generalized to the case of two matrixes $A, B \in \mathbb{R}_M$. If $A^{-1}B \in \mathbb{Q}_M$, then $D \in \mathbb{R}_M$ is a common left divisor of A and B if $A = DP$ and $B = DQ$, with $P, Q \in \mathbb{Z}_M$.

Given matrix $A \in \mathbb{Q}_M$, any ordered pair of left coprime matrixes (H, K) of $\mathbb{Z}_M$ with $\det(H) \neq 0$, such that $A = H^{-1}K$, is called a left coprime factorization (lcf) of A. It is easy to see that, given matrixes $A, B \in \mathbb{R}_M$ with $A^{-1}B \in \mathbb{Q}_M$, if $D = \text{gcld}(A, B)$, it is $D = AH^{-1} = BK^{-1}$ where (H, K) is a lcf of $A^{-1}B$.

Result A.5 [10]: Any matrix $A \in \mathbb{Q}_M$ has an lcf. Given an lcf (H, K) of A, an ordered pair (H_i, K_i) of matrixes of $\mathbb{Z}_M$ is another lcf of A if and only if there exists a unimodular matrix $U_i \in \mathbb{Z}_M$ such that $H_i = U_iH$ and $K_i = U_iK$.

In order to find the left coprime factorization of a full rank matrix $A \in \mathbb{Q}_M$, one can use the following algorythm [10]. Let $U, V \in \mathbb{Z}_M$ be unimodular matrixes such that UAV is in Smith–McMillan normal form:

$$UAV = S_b^{-1}S_a, \quad S_b = \text{diag}\{b_1, b_2, \cdots, b_M\},$$
$$S_a = \text{diag}\{a_1, a_2, \cdots, a_M\} \qquad \text{(A.5)}$$

with $\{b_i\}$ and $\{a_i\}$ satisfying all the properties (A.4). Then $(H = S_bU, K = S_aV^{-1})$ is an lcf of A.

Result A.5 straightforwardly implies that all the lcf (H_i, K_i) of a given matrix A, share the same value of $|\det(H_i)|$ and of $|\det(K_i)|$. The next corollary shows how to obtain such values when A is a full-rank 2×2 matrix of rational numbers, without explicitly calculating an lcf of A.

Corollary A.1: Given any lcf (H, K) of a full-rank matrix $A \in \mathbb{Q}_2$, it is

$$|\det(H)| = \text{den}(A) \cdot \text{den}(\text{den}(A) \cdot \det(A)) \qquad \text{(A.6)}$$
$$|\det(K)| = \text{den}(A) \cdot \det(A) \cdot \text{den}(\text{den}(A) \cdot \det(A)) \qquad \text{(A.7)}$$

Proof: Let S_a and S_b be the diagonal matrixes of (A.5), with $H = S_bU$, $K = S_aV^{-1}$, U and V unimodular. Then $|\det(H)| = \det(S_b) = b_1b_2$. Furthermore, it is $|\det(A)| = |\det(UAV)| = \det(S_a)/\det(S_b)$ and $b_1 = \text{den}(A)$ (by Result A.4). Hence, $\text{den}(A) \cdot \text{den}(\text{den}(A) \cdot \det(A)) = b_1 \cdot \text{den}(b_1 \cdot (a_1/b_1) \cdot (a_2/b_2)) = b_1b_2 = |\det(H)|$, since (a_2, b_2) [as well as (a_1, b_2)] are coprime.

Equation (A.7) derives straightforwardly from (A.6) and equality $K = HA$. ■

Corollary A.1, an original contribution of this work, shows its practical usefulness in Section II-A for determining the index of a lattice in the sum of two lattices.

Corollary A.2: Given matrix $A \in \mathbb{Q}_M$, for any ordered noncoprime pair (L, M) of matrixes of $\mathbb{Z}_M$ such that $A = L^{-1}M$, and for any lcf (H, K) of A, it is

$$|\det(L)| > |\det(H)| \text{ and } |\det(M)| > |\det(K)| \qquad \text{(A.8)}$$

Proof: The result directly follows from the noncoprimeness of (L, M) and from Result A.5. ■

Acknowledgment

The authors thank the Referees for their comments and criticism, which truly helped toward an effective presentation of the work.

References

[1] R. E. Crochiere and L. Rabiner, "Interpolation and decimation of digital signals: A tutorial review," *Proc. IEEE*, vol. 69, pp. 300–331, Mar. 1981.

[2] E. Dubois, "The sampling and reconstruction of time-varying imagery with applications in video systems," *Proc. IEEE*, vol. 73, pp. 502–522, Apr. 1985.

[3] R. M. Mersereau and T. C. Speake, "The processing of periodically sampled multidimensional signals," *IEEE Trans. Acoust., Speech, Signal Processing*, vol. ASSP-31, pp. 188–194, Feb. 1983.

[4] J. W. S. Cassels, *An Introduction to the Geometry of Numbers*. Berlin: Springer, 1959.

[5] C. G. Lekkerkerker, *Geometry of Numbers*. Groningen: Wolsters-Noordhoff, 1969.

[6] V. Kucera, *Discrete Linear Control: The Polynomial Equation Approach*. New York: Wiley, 1979.

[7] H. Cohn, *Advanced Number Theory*. New York: Dover, 1980.

[8] M. Newman, *Integral Matrices*. New York: Academic, 1972.

[9] T. A. Ramstad, "Digital methods for conversion between arbitrary sampling frequencies," *IEEE Trans. Acoust., Speech, Signal Processing*, vol. ASSP-32, pp. 577–591, June 1984.

[10] M. Vidyasagar, *Control System Synthesis: A Factorization Approach*. Cambridge: The MIT Press, 1985.

[11] T. Chen and P. P. Vaidyanathan, "Some fundamental issues in multidimensional multirate signal processing," *IEEE Trans. Signal Processing*, vol. 41, pp. 1035–1047, Mar. 1993.

[12] T. Chen and P. P. Vaidyanathan, "Recent developments in multidimensional multirate systems," *IEEE Trans. Circuits Syst. Video Technol.*, to be published.

[13] G. M. Cortelazzo and R. Manduchi, "On the determination of all the sublattices of preassigned index and its application to multidimensional subsampling," *IEEE Trans. Circuits Syst. Video Technol.*, to be published.

[14] R. F. W. Pease and J. O. Limb, "Exchange of spatial and temporal resolution in television coding," *Bell Syst. Tech. J.*, pp. 191–200, Jan. 1971.

[15] P. MacMullen, "Convex bodies which tile space by translations," *Mathematika*, vol. 27, pp. 113–121, 1980.

[16] P. Siohan, "2-D FIR filter design for sampling structure conversion," *IEEE Trans. Circuits Syst. Video Technol.*, vol. 1, pp. 337–350, Dec. 1991.

[17] Y. Neuvo, D. Cheng-Yu, and S. K. Mitra, "Interpolated finite impulse response filters," *IEEE Trans. Acoust., Speech, Signal Processing*, vol. ASSP-32, pp. 563–570, June 1984.

[18] T. Saramäki, Y. Neuvo, and S. K. Mitra, "Design of computationally efficient interpolated FIR filters," *IEEE Trans. Circuits Syst.*, vol. 35, pp. 70–87, Jan. 1988.

[19] R. Ansari and S. Lee, "Two-dimensional non-rectangular interpolation, decimation, and filter banks," in *Proc. ICASSP 88*, New York, NY, Apr. 1988.

[20] E. Viscito and J. P. Allebach, "The analysis and design of multidimensional FIR perfect reconstruction filter banks for arbitrary sampling lattices," *IEEE Trans. Circuits Syst.*, vol. 38, pp. 29–41, Jan. 1991.
[21] A. Knoll, "Filter design for the interpolation of highly subsampled pictures," *Signal Processing: Image Communication*, vol. 3, pp. 239–248, 1991.
[22] T. Saramäki and Y. Neuvo, "A class of FIR Nyquist (*N*th-band) filters with zero intersymbol interference," *IEEE Trans. Circuits Syst.*, vol. CAS-34, p. 1182–1190, Oct. 1987.
[23] A. Biasiolo, G. Cortelazzo, and G. A. Mian, "Computer aided design of multidimensional FIR filters for video appications," *IEEE Trans. Consumer Electron.*, vol. 35, pp. 290–296, Aug. 1989.
[24] J. Hu and L. Rabiner, "Design techniques for two-dimensional digital filters," *IEEE Trans. Audio Electroacoust.*, vol. AU-20, pp. 249–257, Oct. 1972.
[25] L. Rabiner and B. Gold, *Theory and Application of Digital Signal Processing*. Englewood Cliffs, NJ: Prentice Hall, 1975.
[26] Y. Kamp and J. P. Thiran, "Chebysev approximation for two-dimensional nonrecursive digital filters," *IEEE Trans. Circuits Syst.*, vol. CAS-22, pp. 208–218, Mar. 1975.
[27] B. Barbero and M. Muratori, Centro ricerche RAI, Torino, Italy, private communication.
[28] V. Ouvrard and P. Siohan, "Design of two-dimensional video filters with spatial constraints," in *Proc. EUSIPCO 92*, Brussels, Belgium, Aug. 1992.
[29] J. K. Liang, R. J. P. De Figueredo and F. C. Lu, "Design of optimal nyquist, partial response, *N*th band, and non-uniform tap spacing FIR digital filters using linear programming techniques," *IEEE Trans. Circuits Syst.*, vol. CAS-32, pp. 386–392, Apr. 1985.
[30] H. Samueli, "On the design of optimal equiripple FIR digital filters for data transmission applications," *IEEE Trans. Circuits Syst.*, vol. 35, pp. 1542–1546, Dec. 1988.
[31] G. Tonge, "Three-dimensional filters for television sampling," *IBA Experimental and Development*, Report No. 112/81.
[32] D. E. Pearson, *Transmission and Display of Pictorial Information*. London: Pentech, 1975.
[33] C. C. MacDuffee, *The Theory of Matrixes*. New York: Chelsea, 1946.
[34] M. Renfors, "Multi-dimensional sampling structure conversion with one-dimensional *N*th-band filters," in *Proc. IEEE Int. Symp. on Circuits and Systems*, Portland, OR, May 1989.

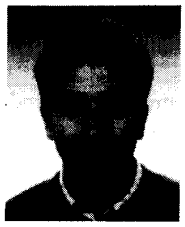

Roberto Manduchi was born in Padova, Italy, in 1965. He received the Laurea in electronics engineering and the Ph.D. degree in telecommunications engineering from the University of Padova in 1989 and 1993, respectively.

He is currently with the Department of Electrical Engineering and Computer Science of the University of California, Berkeley, CA, as a Visiting Scholar. His research interests concern signal processing applied to television and computer vision.

Guido M. Cortelazzo was born in Padova, Italy, in 1952. He received the Laurea degree in electronics engineering from the University of Padova in 1976, and the M.S. and Ph.D. degrees in electrical engineering from the University of Illinois, Urbana-Champaign, IL, in 1980 and 1984, respectively.

In 1982 he was with the University of Padova as a Ricercatore. From 1983 to 1986 he was with M/A-COM Linkabit Inc., San Diego, CA. Since 1987 he has been with the Dipartimento di Elettronica e Informatica of the University of Padova as an Associate Professor. His professional interests concern the area of digital signal processing, image processing, and computer vision.

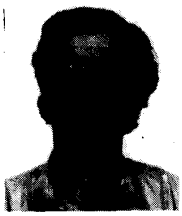

Gian Antonio Mian was born in Padova, Italy, in 1942. He received the Laurea degree in electronics engineering from the University of Padova in 1966.

Since 1968 he has been with the Dipartimento di Elettronica e Informatica of the University of Padova, where he is currently Associate Professor of Digital Signal Processing. His main research interests are in the area of digital filtering and speech and image processing.